Journal of Photochemistry, 6 (1976/77) 23 - 34

THE ULTRA-VIOLET ABSORPTION SPECTRUM OF GASEOUS NITROUS ACID

R. A. COX and R. G. DERWENT
Environmental and Medical Sciences Division, A.E.R.E., Harwell, OX11 ORA (Gt. Britain)
(Received April 15, 1976)

Summary

The ultra-violet absorption spectrum of gaseous nitrous acid was quantitatively examined over the wavelength range 200 - 400 nm. In addition to the diffuse bands between 310 and 380 nm previously reported in the literature, an intense, broad absorption maximum was found at 215 nm.

The absorption cross-sections reported here for 310-380 nm are about a factor of five to six times the previously accepted values. The quantum yield of OH radical production from the photolysis of nitrous acid at 365 ± 5 nm was found to be (0.92 ± 0.16).

The implications of these measurements for the atmospheric chemistry of nitrous acid are discussed.

Introduction

The formation of nitrous acid has been proposed in the lower and upper atmosphere, mainly as a result of the three-body combination process (1) of OH radicals with nitric oxide:

$$OH + NO + M = HONO + M \quad (1)$$

Although it is widely accepted that the photolytic dissociation (2) is the major sink for HONO there is little experimental information on the absorption cross-section and dissociation quantum yield of nitrous acid to enable an accurate calculation of the photodissociation rate:

$$HONO + h\nu = OH + NO \quad (2)$$

The diffuse absorption bands due to HONO have been observed in gaseous mixtures of NO, NO_2 and water vapour, in the spectral region 300 - 400 nm [1]. These bands have been qualitatively analyzed by King and Moule [2] in some detail. Asquith and Tyler [3] have estimated the decadic extinction coefficient at 368 nm to be in the range 50 - 150 l mol^{-1} cm^{-1}. Expressed

according to the Beer–Lambert law in exponential form (i), this corresponds to an absorption cross-section, σ, of between 1.9×10^{-19} and 5.7×10^{-19} cm^2:

$$\ln \frac{I_0}{I} = \sigma n l \qquad \text{(i)}$$

Johnston and Graham [4] have quantitatively analyzed these diffuse bands between 300 and 400 nm due to HONO by assuming complete thermodynamic equilibrium in mixtures containing NO, NO_2 and water vapour. Considerable corrections were required for the underlying absorption components due to the NO_2 and N_2O_3 present. Their tabulated cross-section at 368 nm of 1.23×10^{-19} cm^2 is well below the lower limit quoted by Asquith and Tyler [3]. Recently, we have described a method for the preparation and quantitative analysis of mixtures containing gaseous nitrous acid in air at 1 atmosphere pressure [5]. Although both NO and NO_2 are unavoidably present, stable concentrations and accurate analyses for HONO can be obtained under conditions far removed from the $NO–NO_2–H_2O–HONO$ equilibrium. This system has been used to study the photolysis of nitrous acid [5] and the reactions of OH radicals [6]. A comparison of the relative dissociation rates of NO_2 and HONO in the wavelength range 330 - 380 nm indicated that the HONO absorption cross-section was within the limits quoted by Asquith and Tyler [3].

In the present work, the ultra-violet absorption spectrum of gaseous HONO, prepared by this new method, has been examined in an attempt to resolve these current ambiguities. In addition to measurements in the 300 - 400 nm region, we report a new absorption band of HONO in the 200 - 265 nm region. Experiments designed to determine the quantum yield of OH production from photodissociation of HONO at 368 nm are also described. The implications of these measurements for the lifetime of nitrous acid in the atmosphere are discussed.

Experimental

The methods for preparation and analysis of mixtures containing HONO have been reported before [5] and only a brief description will be given here. Mixtures of nitric oxide, nitrogen dioxide and nitrous acid in nitrogen were prepared by collecting the "nitrous fumes" from the reaction of sulphuric acid with a dilute solution of sodium nitrite. The reagents, 25 ml 10% H_2SO_4 and 75 to 150 ml 0.1 *M* $NaNO_2$ were placed in a 250 ml PTFE-coated flask. Nitrogen at 10 - 15 l/min was passed over the mixed solutions which were gently agitated with a magnetic stirrer. Gaseous HONO, together with some NO and NO_2, volatilized into the N_2 stream and the gas mixture was collected and stored at atmospheric pressure and room temperature (295 ± 2 K) in a 250 l bag constructed of Tedlar film (du Pont Ltd). The gas mixtures also contained water vapour at approximately 30% of its saturated vapour pressure at room temperature.

The concentrations of HONO, NO and NO_2 were measured by the ozone-chemiluminescence technique using a commercial "NO_x" analyzer (Thermo-electron Corp. Model 12A). The instrument measured both NO and NO + NO_2 + HONO directly; the latter measurement involved passing the sample gas through a stainless-steel converter at 1000 K where both NO_2 and HONO were quantitatively decomposed to NO. Gaseous nitrous acid was efficiently removed from the sample gas by a miniature bubbler containing dilute aqueous NaOH, and this allowed HONO to be determined by difference. The analyzer response was calibrated using a standard mixture containing 117.5 ± 5 p.p.m. (1 p.p.m. = 2.43×10^{13} molecules/cm^3 at the mean temperature and pressure during these experiments) nitric oxide in nitrogen, as determined by gas-phase titration against a constant ozone source. The ozone concentration was measured both by ultra-violet absorption at 255 nm using $[O_3] = 1.12 \times 10^{-18}$ cm^2 [7] and by the neutral KI colorimetric method [8].

The gas mixtures used for the absorption measurements contained between 220 p.p.m. and 430 p.p.m. total NO_x (= HONO + NO + NO_2). When initially prepared, nitrous acid comprised at least 50% of the total NO_x with 20 - 40% NO and 10 - 20% NO_2. On standing, nitrous acid decomposed slowly to NO and NO_2. At typical HONO concentrations (150 p.p.m.), the decomposition rate was approximately 10 - 15 p.p.m./h.

Two absorption cells were used in this work with path lengths of 0.55 m and 0.30 m. The cells were constructed from Pyrex tubing with planar fused-quartz end windows cemented in place. The gas mixtures were passed through the cell by connecting it in series with the reservoir and chemiluminescence analyzer. The analyzer drew a constant flow of approximately 17 ml/s which gave a residence time of 40 sec in the larger absorption cell. Under these conditions, no detectable decomposition of nitrous acid occurred in the cell.

Two light sources were employed in these studies; a tungsten–halogen lamp (Atlas, 50 W) was used for the wavelength range 300 - 400 nm and a deuterium lamp (Manuf. Supply Ltd, 35 W) for the entire 200 - 400 nm region. Both sources were operated using constant voltage–constant current stabilized d.c. supplies. The collimated light beam passed through the absorption cell and was focused on the inlet slit of an 0.5 m Czerny–Turner monochromator (Spex). The 1200 groove mm^{-1} grating was blazed at 750 nm. The dispersed radiation was detected using a photomultiplier (EMI, 9526A) mounted on the exit slit. The photomultiplier output was digitized and fed to a pulse counter where the accumulated counts gave a measure of the resolved light transmitted through the absorption cell. In order to correct for short-term variations in the light-source output, the counting period was controlled using a reference photomultiplier, which monitored the light beam entering the absorption cell through a 311 nm interference filter. The output of the reference photomultiplier was similarly digitized and fed to a second pulse counter, which fed an "inhibit" signal to the first counter after the accumulation of a preset number of counts in the reference channel. The

sensitivity of the reference channel was adjusted to give counting periods of about 5 sec; 5 separate count readings were taken for each intensity measurement and they usually agreed to within ±0.01%. Absorbances were determined from the average readings with and without absorbing material present in the cell, I^{λ} and I_0^{λ} respectively. In practice, the smallest absorption that could be detected was limited by drift in the system between measurements of I^{λ} and I_0^{λ}. This was approximately 0.1% which is equivalent to an apparent cross-section of approximately 5×10^{-21} cm^2 for HONO at the concentrations used.

At most wavelengths, a correction for absorption by nitrogen dioxide was required. This correction was made on the basis of the chemiluminescence analysis of the HONO, NO and NO_2 concentrations in each mixture and the absorption cross-sections for NO_2 given by Johnston and Graham [4]. The NO_2 content of the mixtures was also checked by its absorption at 400 nm where absorption due to HONO was insignificant. The correction normally amounted to approximately 50% of the observed absorptions at "off peak" wavelengths in the centre of the near ultra-violet HONO absorption; at the absorption maxima and in the 200 - 265 nm absorption band, the absorption component due to NO_2 was much less. Corrections for absorption by nitric oxide in the γ bands at 215 and 205 nm were also applied using data from Calvert and Pitts [9]. On the basis of the equilibrium constants given by Leighton [10], absorptions due to N_2O_3 and N_2O_4 were expected to be negligible in the present work. The equilibrium concentrations of these oxides were in the range 0.001 to 0.018 p.p.m. and 0.010 to 0.34 p.p.m. respectively, *i.e.* a factor of $>10^3$ less than the concentrations of NO_2 and HONO. The accumulated error in the HONO cross-sections due to instrumental drift between the measurements of I^{λ} and I_0^{λ}, analytical errors and uncertainties resulting from the correction for absorptions by NO_2 and NO, was equivalent to $\pm 5 \times 10^{-20}$ cm^2 over the wavelength range investigated.

The wavelengths were manually selected on the monochromator always from the low wavelength side. The wavelength selector was calibrated using a mercury arc, the greatest deviation being 0.5 nm with the indicated wavelength slightly higher than the true value. Slit widths were 0.1 to 0.25 mm giving a resolution significantly better than 0.1 nm.

Photolysis experiments were carried out using a 27 ml cylindrical Pyrex cell with planar quartz end windows, which was irradiated by a filtered beam from a high pressure mercury arc (Mazda, ME/D 250 W). The radiation passing the glass filters (5 mm Pyrex + 3 mm Chance 0X1) was predominantly centred about the 365 nm mercury line. The gas mixtures flowed through the cell in the same manner as for absorption measurements and the photolysis rates were measured from the changes in concentration of NO and NO_2 upon photolysis for a few seconds.

TABLE 1

The measured absorption cross-sections, σ, in cm^2 of gaseous HONO in the wavelength range 200 - 400 nm

200 - 310 nm region

λ	$\sigma \times 10^{20}$	λ	$\sigma \times 10^{20}$
200	125	260	8
205	185	265	4
210	295	270	2
215	425	275	<0.4
220	177	280	<0.4
225	140	285	<0.4
230	104	290	<0.4
235	68	295	<0.4
240	42	300	<0.4
245	28	305	<0.4
250	18	310	<0.4
255	11		

311 - 400 nm region

λ	$\sigma \times 10^{20}$	λ	$\sigma \times 10^{20}$	λ	$\sigma \times 10^{20}$	λ	$\sigma \times 10^{20}$	λ	$\sigma \times 10^{20}$
311	<0.4	331	18	351	24	371	19	391	3
312	<0.4	332	21	352	28	372	29	392	1
313	<0.4	333	13	353	47	373	15	393	3
314	2	334	14	354	56	374	12	394	<0.4
315	1	335	19	355	29	375	17	395	<0.4
316	1	336	12	356	20	376	17	396	<0.4
317	5	337	13	357	22	377	13	397	<0.4
318	4	338	27	358	19	378	12	398	<0.4
319	3	339	23	359	17	379	16	399	<0.4
320	7	340	24	360	17	380	22	400	<0.4
321	10	341	49	361	18	381	22		
322	6	342	26	362	16	382	21		
323	12	343	23	363	17	383	30		
324	3	344	18	364	21	384	33		
325	22	345	24	365	23	385	21		
326	5	346	20	366	27	386	9		
327	18	347	20	367	56	387	8		
328	11	348	23	368	56	388	5		
329	18	349	17	369	27	389	3		
330	26	350	27	370	25	390	2		

Results and discussion

Absorption spectrum of nitrous acid

Table 1 shows a summary of the measured absorption cross-sections of gaseous nitrous acid from 200 to 400 nm corrected for contributions due to

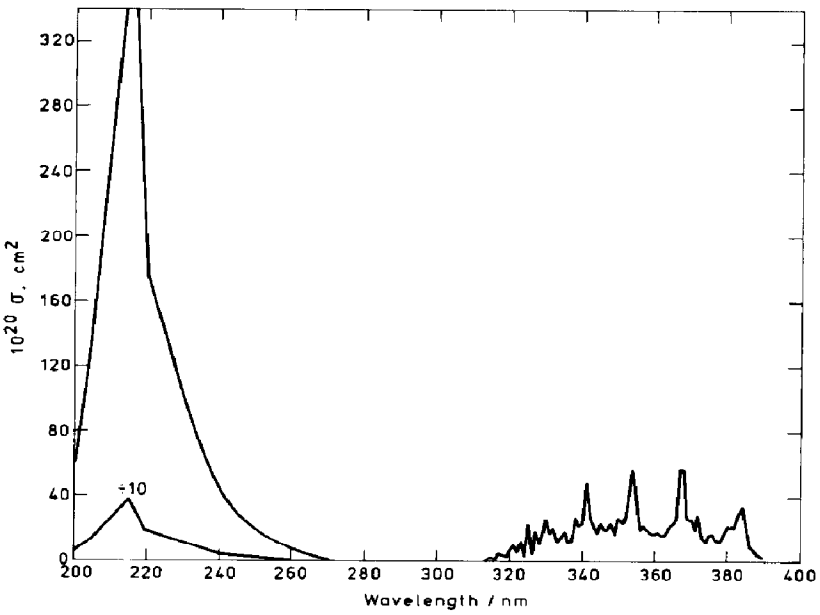

Fig. 1. The absorption spectrum of gaseous nitrous acid from 200 to 400 nm.

NO_2 and NO. The data for the 200 - 320 nm region are mean values from two series of experiments: path length 0.55 m; HONO concentration between 150 p.p.m. and 190 p.p.m. For the 320 - 400 nm region, the mean values derived from two to four measurements at each wavelength are given; path lengths of 0.3 and 0.55 m and HONO concentrations in the range 85 to 190 p.p.m. were employed. The spectrum is illustrated in Fig. 1. The previously reported diffuse banded structure is clearly evident in the 320 - 390 nm region. The positions of the absorption maxima are compared in Table 2 with those observed by King and Moule [2] in their high resolution study using nitrous acid prepared *in situ* from mixtures of NO, NO_2 and water vapour. Generally, the agreement is quite acceptable within the rather limited resolution of our measurements at 1 nm intervals.

The absorption cross-sections in the wavelength range 275 - 310 nm fall to the lower limit for detection in our system. Below 275 nm we observe a broad absorption band with peak intensity at 215 nm; this feature has not been reported previously. However, similar broad absorption bands with maxima near 220 nm have been reported for the organic esters of HONO, methyl nitrite and t-butyl nitrite [9]. The spectra of these compounds also exhibit a series of diffuse bands between 300 and 400 nm, similar to those observed for nitrous acid.

Figure 2 shows a Beer–Lambert plot of the absorption due to HONO at 220 nm and 354 nm. The concentration of HONO (and NO and NO_2) was varied by dilution of the gas mixture flowing through the absorption cell with a controlled flow of high purity N_2. Within the experimental scatter both plots pass through the origin and show no significant deviations from linearity. This provides justification of the assumption that absorptions due

TABLE 2

Wavelengths (nm) in air of absorption maxima in the ultra-violet spectrum of nitrous acid

King and Moule	This work
314.3	314
317.8	317
320.7	321
323.8	323
327.7	327
330.7	330
334.6	335
338.7	338
341.7	341
346.1	345
350.8	350
353.8	354
357.6	357
364.6	364
368.2	368
371.5	372
384.0	384

to N_2O_3 and N_2O_4 were negligible, since the equilibrium concentrations of these oxides are proportional to $[NO] \times [NO_2]$ and $[NO_2]^2$, respectively [10], and would decrease proportionately more rapidly with dilution. The slopes give $\sigma_{220} = 177 \pm 18 \times 10^{-20}$ cm^2 and $\sigma_{354} = 67 \pm 7 \times 10^{-20}$ cm^2 for the HONO cross-sections. The corresponding cross-sections for methyl nitrite at the maxima in the two respective absorption regions are 420×10^{-20} cm^2 and 31×10^{-20} cm^2 at 340 nm [9]. The similarities in the absorption intensities for HONO and CH_3ONO in the respective bands indicate that the same electronic transitions are involved.

The absorption cross-section at 354 nm is approximately a factor six higher than given by Johnston and Graham [4]. This discrepancy was apparent throughout the 320 - 400 nm absorption region, the mean ratios calculated from comparison of the individual cross-sections at 1 nm intervals were 5.6 (320 - 329 nm), 6.2 (340 - 359 nm), 6.3 (360 - 379 nm) and 4.3 (380 - 393 nm). However, at 368 nm, our value of $\sigma = 56 \pm 5 \times 10^{-20}$ cm^2 is in excellent agreement with the upper limit given by Asquith and Tyler [3], 57×10^{-20} cm^2.

Comparison of the results in Table 1 with the tabulation of Johnston and Graham [4] shows slight differences between the wavelengths in air of the absorption maxima. This is no doubt partly caused by the wavelength interval, 1 nm, being too large to completely define the spectral features and partly due to differences in the resolution of the two optical systems. We are unable to explain, however, the large numerical factor separating the

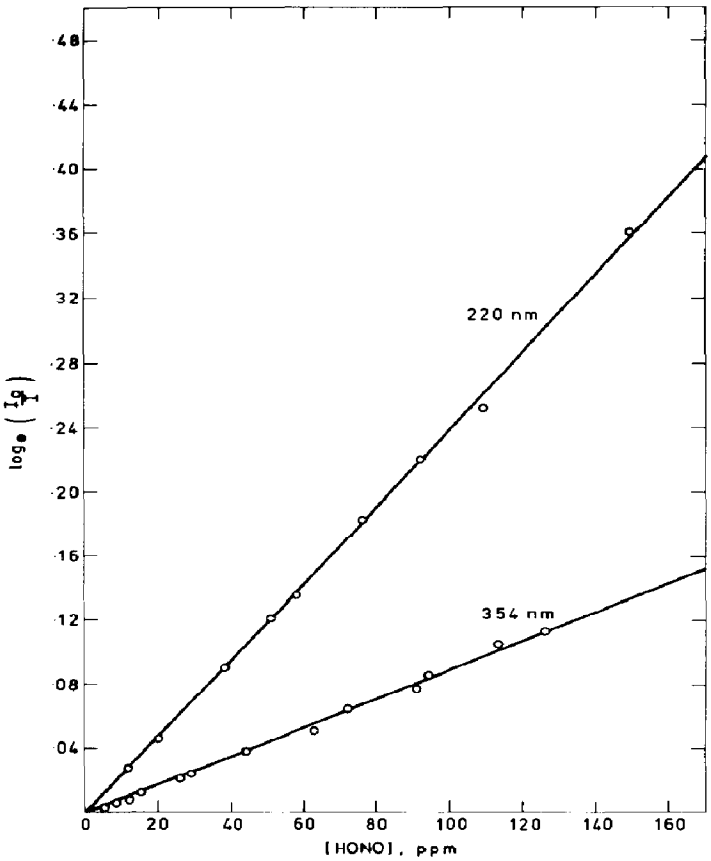

Fig. 2. Beer–Lambert law plots for absorptions due to HONO at 220 nm and 354 nm.

measured cross-sections in the two investigations. Certainly, we cannot accommodate an error of this magnitude in our measurements and we can only suggest that complete thermodynamic equilibrium in the $NO–NO_2–H_2O–HONO$ system was not reached in the experiments of Johnston and Graham [4].

Quantum yield for photodissociation of nitrous acid at 365 ± 5 nm

The quantum yield, $\Phi(HONO)$, for the dissociation of HONO was estimated by comparison of the rates of light absorption by NO_2 and HONO, (k_a), with their measured rates of decomposition (k_d) in the 27 ml photolysis cell. From a knowledge of the quantum yield for photodissociation of NO_2 at the appropriate wavelength, $\Phi(HONO)$ can be determined from:

$$\Phi(HONO) = \Phi(NO_2) \times \frac{k_d^{HONO}}{k_d^{NO_2}} \times \frac{k_a^{NO_2}}{k_a^{HONO}} \qquad \text{(ii)}$$

The output of the high pressure mercury arc + filter combination employed in the photolysis experiments was monitored at 1 nm intervals between 360 and 370 nm using the monochromator–photomultiplier combination. From

TABLE 3

Photodissociation of nitrous acid

Initial concentrations (p.p.m.)*			Photolysis time (sec)	d[NO]/dt	d[NO_2]/dt	k_d^{HONO} ($s^{-1} \times 10^2$)
HONO	NO	NO_2		(p.p.m. $s^{-1} \times 10^2$)		
3.85	0.19	0.15	1.43	2.63	2.18	0.740
3.85	0.19	0.15	3.31	2.40	2.34	0.684
9.84	0.80	0.58	3.26	5.81	5.43	0.675
22.90	2.22	1.28	1.47	13.83	11.53	0.698
22.90	2.22	1.28	3.31	12.99	11.33	0.661

*In N_2 + O_2 (2:1) at atmospheric pressure and 295 K.

the absorption cross-sections for HONO measured here and those for NO_2 given by Johnston and Graham [4], the relative photon absorption rate, the ratio $k_a^{NO_2}/k_a^{HONO}$, was found to be 2.27 ± 0.36.

The photodissociation rate of HONO was determined from the measured rates of formation of NO and NO_2 in the photolysis of HONO–NO–NO_2 mixtures diluted in N_2 + O_2 as described previously [5]. The rate data were corrected for the small contribution from the photolysis of NO_2 present. k_d^{HONO} was calculated assuming the following mechanism for the photolysis of HONO:

HONO + $h\nu$	= OH + NO	k_d^{HONO}	
OH + NO + M	= HONO + M		(1)
OH + NO_2 + M	= $HONO_2$ + M		(3)
OH + HONO	= H_2O + NO_2		(4)

with $k_1 = k_3 = 1.7\ k_4$ [11]. The results, which are summarized in Table 3, gave a mean value of $k_d^{HONO} = (0.69 \pm 0.03) \times 10^{-2}\ s^{-1}$.

The photolysis of NO_2–N_2–O_2 mixtures was carried out with the same optical geometry as for the HONO photolyses, and the production of nitric oxide monitored. The photolysis of nitrogen dioxide proceeds by the following mechanism under the conditions employed:

NO_2 + $h\nu$	= NO + $O(^3P)$	$k_d^{NO_2}$	
O + NO_2	= NO + O_2		(5)
O + NO_2 + M	= NO_3 + M		(6)
O + NO + M	= NO_2 + M		(7)
O + O_2 + M	= O_3 + M		(8)
NO + NO_3	= NO_2 + NO_2		(9)
NO_3 + NO_2	⇌ N_2O_5		(10)

TABLE 4

Photodissociation of nitrogen dioxide

Initial concentrations (p.p.m.)*			Photolysis time (sec)	ΔNO (p.p.m.)	
NO	NO_2	O_2		Measured	Computed
0.381	9.04	0	1.41	0.371	0.355
0.491	8.81	12.5		0.350	0.343
0.510	8.71	25.5		0.343	0.339
0.526	8.69	155.5		0.334	0.334
0.560	8.63	294.5		0.325	0.328
0.590	8.60	440.5		0.320	0.323
0.600	8.59	786.5		0.312	0.316
0.612	8.55	1554.5		0.290	0.300

*In N_2 at atmospheric pressure and 295 K.

$$NO + O_3 = NO_2 + O_2 \quad (11)$$

$$NO_2 + O_3 = NO_3 + O_2 \quad (12)$$

Because the equilibrium according to reaction (10) is not achieved during the time-scale of our photolyses, steady state analyses cannot strictly be applied. Solution of the differential equations describing the photolysis of NO_2 was carried out by numerical integration using the Harwell computer program CHEK [12]. Current consensus values of the rate constants k_5 to k_{12} were employed [13, 14]. $k_d^{NO_2}$ was varied to give best fit to the measured production of NO, ΔNO. Table 4 shows the experimental results together with the results of the computations using $k_d^{NO_2} = (1.7 \pm 0.1) \times 10^{-2}$ s^{-1}, which gave the best fit.

Substitution of the relevant quantities in eqn. (ii) gives: $\Phi(HONO) = (0.92 \pm 0.16)\ \Phi(NO_2)$. It can be considered well established [13] that $\Phi(NO_2)$ is unity from 398 to 244 nm. When the systematic error involved in the neglect of photolysis occurring in our system outside the 360 - 370 nm region, and the experimental errors in the determination of k_d and k_a are taken into account, it is probable that the quantum yield for photodissociation of HONO is also unity at 365 ± 5 nm.

Atmospheric chemistry

The atmospheric chemistry of nitrous acid is dominated by two competing sink processes. These are photolysis by solar radiation between 200 and 400 nm and destruction by OH radicals. The importance of the latter can be estimated from the OH + HONO rate constant recently determined as 6.6×10^{-12} cm^3 $molecule^{-1}$ s^{-1} at 296 K [11] and computed OH radical concentrations in the troposphere and stratosphere. These concentrations lie largely in the range (1.0 to 10) $\times 10^6$ molecule/cm^3, indicating first order removal rate coefficients of the order of (7.0 to 70) $\times 10^{-6}$ s^{-1}.

TABLE 5

Estimated photolysis rate coefficients in $(second)^{-1}$ for nitrous acid at various altitudes and solar zenith angles.

Zenith angle (degrees)	0 - 5 km $\times 10^3$	15 - 20 km $\times 10^3$	30 - 35 km $\times 10^3$	45 - 50 km $\times 10^3$
10	2.7	2.7	2.8	3.1
30	2.5	2.7	2.8	3.1
60	1.7	2.8	2.8	3.1
80	0.4	1.7	2.7	3.0

These rate coefficients were calculated from the measured absorption cross-sections and the solar photon flux at each altitude. This solar photon flux was estimated by the method of Kockarts [15], using the data reviewed by Ackerman. Molecular oxygen absorption cross-sections were taken from Hudson and Mahle [16]. Tropospheric effects were evaluated by the analysis given by Leighton [10].

The measured absorption cross-sections have been used to calculate the atmospheric photolysis rates of nitrous acid given in Table 5. The estimated rate coefficients fall in the range (3.1 to 0.4) $\times 10^{-3}$ s^{-1} over a wide range of altitudes and solar zenith angles. These photolysis rate coefficients are several orders of magnitude larger than the rate coefficients for all other destruction reactions and clearly demonstrate the importance of photodissociation in the life cycle of nitrous acid.

In the atmosphere, nitrous acid is largely formed by combination of OH radicals with NO (eqn. 1), with the reverse stoichiometry of the photolysis process. Reaction (1) would not therefore appear to represent a net sink for free radicals in the sunlit atmosphere.

Acknowledgement

This work was carried out as part of an air pollution research program sponsored by the Department of the Environment.

References

1 E. H. Melvin and O. R. Wulf, Phys. Rev., 38 (1931) 2294.
2 G. W. King and D. Moule, Can. J. Chem., 40 (1962) 2057 - 2065.
3 P. L. Asquith and B. J. Tyler, Chem. Commun., (1970) 744 - 745.
4 H. S. Johnston and R. Graham, Can. J. Chem., 52 (1974) 1415 - 1423.
5 R. A. Cox, J. Photochem., 3 (1974) 175 - 188.
6 R. A. Cox, Int. J. Chem. Kinet., Suppl. VII (1975) 379.
7 M. Ackerman, in G. Fiocco (ed.), Mesospheric Models and Related Experiments, D. Reidel, Dordrecht, (1971) pp. 149 - 159.
8 B. E. Saltzman, Selected Methods for the Measurement of Air Pollutants, Public Health Service Publication No. 999 - AP - 11, (1965).
9 J. G. Calvert and J. N. Pitts Jr., Photochemistry, Wiley, New York, (1967).

10 P. A. Leighton, Photochemistry of Air Pollution, Academic Press, London (1961).
11 R. A. Cox, R. G. Derwent and P. M. Holt, J. Chem. Soc. Faraday Trans. I, 72 (1976) in press.
12 A. R. Curtis and E. M. Chance, CHEK and CHEKMAT: Two Chemical Reactions Kinetics Programs, A.E.R.E. Report R7345, HMSO, London.
13 D. Hampson and R. F. Garvin, Chemical Kinetics Data Survey VII, Tables of Rate and Photochemical Data for Modelling of the Stratosphere, NBSIR 74-430, N.B.S., Washington, (1974).
14 D. H. Stedman and H. Niki, J. Phys. Chem., 77 (1973) 2604 - 2609.
15 G. Kockarts, in G. Fiocco (ed.), Mesospheric Models and Related Experiments, D. Reidel, Dordrecht, (1971) pp. 160 - 176.
16 R. D. Hudson and Mahle, J. Geophys Res., 77 (1972) 2902 - 2914.